Title
Enriched East Asian oxygen isotope of precipitation indicates reduced summer seasonality in regional climate and westerlies

Journal
Proceedings of the National Academy of Sciences of the United States of America, 117(26)

ISSN
0027-8424

Authors
Chiang, John CH
Herman, Michael J
Yoshimura, Kei
et al.

Publication Date
2020-06-30

DOI
10.1073/pnas.1922602117

Peer reviewed

Enriched East Asian oxygen isotope of precipitation indicates reduced summer seasonality in regional climate and westerlies

John C. H. Chiang[1], Michael J. Herman[1], Kei Yoshimura[2], and Inez Y. Fung[3]

[1] Department of Geography, University of California, Berkeley CA 94720

[2] Atmosphere and Ocean Research Institute, The University of Tokyo, Kashiwa, Chiba 277-8574, Japan

[3] Department of Earth and Planetary Sciences, University of California, Berkeley CA 94720

Corresponding author: John Chiang (jch_chiang@berkeley.edu)

Classification
Physical Sciences: Earth, Atmospheric and Planetary Sciences.

Keywords
Paleoclimate, Monsoon, Westerlies, East Asia.

Author Contributions
JCHC led the design of the study and manuscript writing; MJH led the analysis and contributed to the design and writing; KY contributed the isoGSM2 dataset and provided interpretation and analyses; IYF provided expert interpretation and contributed to writing.

This PDF file includes:
Main Text
Figures 1 to 4

Abstract

Speleothem oxygen isotope records over East Asia reveal apparently large and rapid paleoclimate changes over the last several hundred thousand years. However, what the isotopic variation actually represent in terms of the regional climate and circulation is debated. We present an answer that emerges from an analysis of the interannual variation in amount-weighted annual $\delta^{18}O$ of precipitation over East Asia as simulated by an isotope-enabled model constrained by large-scale atmospheric reanalysis fields. ^{18}O-

enriched years have reduced summer seasonality both in terms of precipitation isotopes and in the large-scale circulation. Changes occur between June and October, where the $\delta^{18}O$ of precipitation ($\delta^{18}O_p$) transitions from the isotopically heavier winter to the lighter summer regime. For ^{18}O-enriched years, this transition is less pronounced. Variations in precipitation amount alone are insufficient to explain the amount-weighted annual $\delta^{18}O_p$ between ^{18}O-enriched and depleted years. Reduced summer seasonality is also expressed in the low-level monsoonal southerlies and upper-level westerlies; for the latter, the northward migration across the Tibetan Plateau in the summer is less pronounced. Our result thus implicates the westerlies across the Plateau as the proximate cause of East Asian paleomonsoon changes, and manifested as a modulation of its summer peak.

Significance Statement

Cave oxygen isotope records have revolutionized our understanding of East Asian paleoclimate. However, the climate interpretation of these records has proven controversial, some arguing for substantial swings in monsoon intensity while others suggesting that they do not indicate climate changes over East Asia. A modern-day analog provides an answer: namely, a modulation in the seasonal amplitude of East Asian summer climate and circulation. A strong connection exists with the seasonal migration of the westerlies across the Tibetan Plateau, consistent with dynamical arguments that point to this migration to control East Asian summer monsoon seasonality. Our result thus inserts paleoclimate evidence into the current debate on East Asian summer monsoon dynamics, and in favor of a greater role for the westerlies.

Introduction

Speleothem oxygen isotope ($\delta^{18}O_c$) records over East Asia and other tropical regions have revolutionized our understanding of the global paleomonsoon[1, 2]. However, there remains a basic question of what the calcite oxygen isotopic records represent in terms of regional climate changes, specifically the large-scale circulation. This is particularly true for the East Asian records, even though they are amongst the most studied[3]. Previous interpretations proposed modulation of 'monsoon intensity' through changes to the ratio of summer to winter precipitation[4], variation to the isotopic depletion of moisture advected by convection upstream of the speleothem sites[5, 6, 7], and selection among different moisture source regions[8].

From a dynamical perspective, there are two general approaches to analyzing East Asian climate and its seasonality. Traditionally, East Asia is viewed as a monsoon system - in the summer, differential warming between land and ocean creates pressure differences that in turn drive low-level southerly flows that brings warm moist air from the surrounding oceans into East Asia[9]. Atmospheric heating from convection, especially in the southern reaches of the Tibetan Plateau, provides an important positive feedback[10]. Seasonality is integral to monsoon systems: in the winter, the land-ocean thermal contrast reverses, and northerlies sweep cold and dry air across East Asia.

An alternative viewpoint shifts the focus to tropospheric westerlies. East Asia is sufficiently north to be within the westerly belt even in the early summer, and the Tibetan Plateau provides both a mechanical and thermal obstacle that deflects the westerlies, generating a stationary eddy circulation downstream; the interaction of this circulation with the low-level monsoonal flow generates the rainfall climate over East Asia[11, 12]. The westerly core shifts from south of the Plateau in the winter and spring, to the north of the Plateau in the height of summer, before transitioning back again[13]. Thus, the westerly migration adds its own imprint onto the seasonality of East Asia, noted by Chinese meteorologists since at least the 1950's[14, 15]. Molnar et al. (2010)[12] formalized this view by hypothesizing a correspondence between the seasonal evolution of East Asian summer rainfall with the meridional position of the westerlies.

Here, we present an analysis that describes East Asian climate and large-scale circulation changes when the oxygen-18 isotope composition in precipitation ($^{18}O_p$)

becomes depleted or enriched, derived from an analysis of the latter's interannual variability in an isotope-enabled model simulation (Isotope-incorporated Global Spectral Model version 2 (hereafter isoGSM2)[16]) that simulates modern East Asian rainfall and $\delta^{18}O_p$ with fidelity. The climatological monthly variation of East Asian $\delta^{18}O_p$ in isoGSM2 compares favorably with direct measurements, and performs significantly better than isotope-enabled model simulations used in previous studies of East Asia (SI Appendix, section 1). Moreover, it is able to simulate the interannual variability of warm-season $\delta^{18}O_p$ to the extent that this can be compared to the limited measurements (SI Appendix, section 2). A clear interpretation emerges: years with enriched $^{18}O_p$ over East Asia have reduced amplitudes of the annual cycle, both in $\delta^{18}O_p$ and in the regional large-scale circulation, mainly due to reductions in the magnitudes of the excursions during the summer seasons. We shall refer to this as "reduced summer seasonality", which could mean lower summer peaks (e.g. precipitation) or shallower summer troughs (e.g. $\delta^{18}O_p$). Moreover, we demonstrate a strong link between East Asian $^{18}O_p$ and the meridional position of the westerlies, with enriched values associated with a southward-shifted jet during summer.

Results

a) Interannual variability of amount-weighted annual $\delta^{18}O$ over East Asia

The dominant interannual variation of isoGSM2 amount-weighted annual $\delta^{18}O_p$ over East Asia, extracted through an empirical orthogonal function (EOF) analysis (see Materials and Methods), possesses a mostly uniform sign across East Asia extending from the Bay of Bengal to northeastern China and eastward to the Philippines (figure 1a). Over China, it extends from Hebei province in the northeast to Yunnan province in the southwest (as highlighted by the parallelogram in figure 1a). Interestingly, this region encompasses the key speleothem locations of Hulu, Dongge, and Sanbao caves, as well as several others with strong temporal coherence in the proxy record (filled black dots in figure 1a). Extending this comparison, we reviewed existing speleothem studies over East Asia and marked their location if a record exhibited temporal variations seen in Hulu-Dongge-Sanbao record[17] (SI Appendix, section 3); notably, the cave locations cluster within the parallelogram region (other black dots in figure 1a).

We create an interannual index for $\delta^{18}O_p$ by averaging the amount-weighted annual $\delta^{18}O$ over the parallelogram region (figure 1b, black line; hereafter the ***parallelogram $\delta^{18}O_p$ index***). This index allows us to identify years with enriched and depleted $^{18}O_p$, upon which we form composites to examine their characteristics in terms of seasonal behavior and large-scale circulation. The parallelogram $\delta^{18}O_p$ index is strongly correlated with the principal component of EOF 1 (figure 1b, blue line) ($r = 0.87$, $p < 0.01$), indicating that the interannual variation in amount-weighted annual $\delta^{18}O_p$ within the parallelogram region is coherent and tied to EOF1. Variations in the parallelogram $\delta^{18}O_p$ index are ~2‰ (peak-to-peak), comparable in magnitude to millennial variations of $\delta^{18}O$ in speleothem records[4]. We composite various climate fields for years of higher and lower values of the parallelogram $\delta^{18}O_p$ index (corresponding to ^{18}O-enriched and depleted years, respectively), using ±0.5 standard deviation as the threshold (figure 1b, dashed red lines).

Figure 2a shows the month-to-month variation in rain amount multiplied by $\delta^{18}O_p$ averaged over the parallelogram region, and for $^{18}O_p$-enriched and depleted years. Differences between enriched and depleted years occur exclusively in the warm season, from June through October (JJASO). A similar conclusion is reached if solely $\delta^{18}O_p$ is considered (figure 2b), with $\delta^{18}O_p$ higher across JJASO for enriched years relative to depleted years. Rainfall during enriched years are also somewhat less than for depleted years (figure 2c), and while the differences for each month are not significant (apart from October), rainfall reduction summed over JJASO is significant at $p < 0.01$. The reduced summer precipitation seasonality during enriched years is more clearly shown if month-to-month fluctuations - tied to strong weather variations over East Asia - are filtered out prior to compositing (SI Appendix, section 4 and figure S7c), as is the case for rain amount x $\delta^{18}O_p$ and $\delta^{18}O_p$ (SI Appendix, figure S7a and S7b respectively). Overall, enriched years are so because there is reduced summer seasonality in $\delta^{18}O_p$ - it does not become as isotopically light in the summer as compared to depleted years. Additional analyses of $\delta^{18}O_p$ over the parallelogram region (SI Appendix, section 5) confirm this interpretation.

b) Large-scale circulation changes associated with $\delta^{18}O_p$ variation

Changes to the surface circulation are consistent with the interpretation of reduced summer seasonality for enriched years (figure 3). Warm season east-west pressure contrast between the Asian continent and Western North Pacific is reduced, largely as a result of a weaker and/or eastward-shifted Western Pacific subtropical high (figure 3a, shaded). The vertically-integrated moisture flux into East Asia from the South China Sea is also reduced (figure 3a, vectors). Seasonally, the northward moisture flux over southeastern China is weaker during July-September (figure 3b), a consequence of weaker lower tropospheric meridional winds (figure 3c). Changes in the upper level circulation are also consistent with reduced summer seasonality for enriched years. Enriched years show decreased warm season westerlies to the north of the Plateau and increased to the south of it (figure 3d), indicating a reduced northward migration of the westerlies. We track the latitudinal position of westerlies across Asia centered on the Tibetan Plateau (see Materials and Methods) for enriched years and depleted years (figure 3e); the analysis shows a systematic southward shift of the westerlies across all months from March through December during enriched years, though the difference is significant only for July through October ($p < 0.05$).

There is a robust link between the latitude position of the warm season westerlies and $\delta^{18}O_p$ over the parallelogram region. Correlation of the latitude of the 200mb zonal wind maximum across Asia centered on the Tibetan Plateau (40-140°E) with $\delta^{18}O_p$ averaged over the parallelogram region shows significant correlation for June, July, October and November (SI Appendix, figure S10a). $\delta^{18}O_p$ is generally not associated with the strength of the jet, however (SI Appendix, figure S10b). Furthermore, an objective spatiotemporal analysis method designed to find coupled behavior between fields shows that the leading summertime mode is a pattern with reduced westerlies north of the Plateau and increased westerlies to the south of the Plateau associated with enriched $^{18}O_p$ over the parallelogram region (SI Appendix, section 6(ii) and figure S11). The temporal behavior of this mode is correlated to principal component 1 of the EOF of amount-weighted annual $\delta^{18}O_p$ (figure 1) at $r = 0.92$ ($p < 0.01$), meaning that both analysis methods extracted essentially the same interannual behavior for $\delta^{18}O_p$ over East Asia. The evidence thus suggests robust physical relationships between the large-scale westerly wind and the summertime East Asian $\delta^{18}O_p$.

c) Implications for interpretation of East Asian speleothem records

Wang et al. (2001)[4] proposed "monsoon intensity" (the ratio of winter-to-summer rainfall amounts) as an explanation for speleothem $\delta^{18}O_c$ variations at Hulu cave, observing that wintertime rainfall was isotopically heavy compared to the summer. An alternative hypothesis proposed that East Asian $\delta^{18}O_c$ reflects the isotopic composition of moisture advected from the Indian and Pacific source regions, depleted by Rayleigh fractionation from convection upstream[5, 6, 7]. Recent proxy and modeling evidence lend support to both hypotheses: in particular, Pausata et al. (2011)[6] showed that a Heinrich-like simulation leads to increased $\delta^{18}O_p$ over East Asia because of a decrease in rainfall upstream; and Orland et al. (2015)[18] showed evidence for both monsoon intensity and source changes from a remarkable set of seasonally-resolved speleothem measurements over Northeastern China. Liu et al. (2014)[19] merged the two interpretations by arguing that $\delta^{18}O_c$ variations reflected monsoon intensity through the strength of the low-level monsoonal southerlies and magnitude of rainfall over northeastern China, while also reflecting the continental-scale Asian monsoon rainfall response and its effect on upstream depletion. Finally, differing moisture source regions has also been proposed as an explanation[8].

We estimate the contributions of precipitation anomalies and $\delta^{18}O_p$ variation to the parallelogram $\delta^{18}O_p$ index. Enriched years have a mean amount-weighted annual $\delta^{18}O_p$ anomaly of +0.66 per mil relative to the climatological value, and depleted years -0.71 per mil, a difference of 1.37 per mil. Local precipitation differences (i.e. monsoon intensity) alone contribute only +0.11 per mil to this difference, whereas differences in the $\delta^{18}O_p$ contribute +1.07 per mil; contribution from the covariance between precipitation and $\delta^{18}O_p$ adds the remaining +0.18 per mil. Thus, summertime changes to $\delta^{18}O_p$ contributes to the majority of the difference in amount-weighted annual $\delta^{18}O_p$ between enriched and depleted years. This conclusion mirrors the results of Orland et al. (2015)[18] for their seasonally-resolved speleothem records over northeastern China, who also found that summertime changes to $\delta^{18}O_p$ contribute more to the differences in the $\delta^{18}O_c$ between the early Holocene and Younger Dryas.

To check whether changes to fractionation effects from rainfall processes in the parallelogram region can account for the $\delta^{18}O_p$ change, we plot the $\delta^{18}O$ of precipitable water (hereafter $\delta^{18}O_{pw}$) averaged over the parallelogram region, for enriched and depleted years (figure 2d). The monthly difference between enriched and depleted years for the $\delta^{18}O_{pw}$ quantitatively mirror that for $\delta^{18}O_p$ (SI Appendix, figure S12), indicating that differences between $\delta^{18}O_p$ between enriched and depleted years arise mainly from differences in the $\delta^{18}O$ of moisture advected into the region, and not from fractionation effects of local rainfall. This conclusion is further supported by the lesser significance of rainfall differences (figure 2c) between enriched and depleted years in the parallelogram region.

Thus, understanding the origins of water vapor $\delta^{18}O$ changes over the parallelogram region is key to understanding $\delta^{18}O_p$. Air parcel trajectories into the parallelogram region at 700mb shows that both the origin of the trajectory, and source vapor from the neighboring oceans, exhibit reduced summer seasonality during enriched years relative to depleted years. In climatology, air parcel trajectories originate from southwest of the parallelogram region during June and July, south of the parallelogram region in August, and east of the parallelogram region in September and October (SI Appendix, figure S13); in other words, the origin shifts counterclockwise from the Bay of Bengal in the early summer, to the South China Sea in midsummer, and to the western North Pacific in late summer. The origin point of enriched year trajectories 'sweeps' through these regions faster than for depleted years (figure 4a-c), consistent with our interpretation of reduced summer seasonality. Less water vapor will be sourced from the South China Sea in this case, and precipitable water over the parallelogram region will be isotopically heavier. In addition, the $\delta^{18}O$ of precipitable water over the neighboring ocean regions - Bay of Bengal, South China Sea, and northwestern Pacific - do not become as isotopically light over the summer months for enriched years relative to depleted years (figure 4d-f), again consistent with the interpretation of reduced summer seasonality. A more detailed analysis of air parcel trajectories into the parallelogram region also suggests a role for upstream depletion (SI Appendix, section 8 and figure S14).

The $\delta^{18}O_{pw}$ change is part of a larger pattern of changes with positive anomalies extending from central eastern Asia to the Maritime continent; in the central Pacific, the $^{18}O_{pw}$ is isotopically lighter (figure 4g). This pattern is reminiscent of changes associated with the El Niño Southern Oscillation[20], and indeed there is a significant association between the parallelogram $\delta^{18}O_p$ index and boreal summer El Niño conditions (the parallelogram $\delta^{18}O_p$ index is correlated at r = 0.6 with Niño3.4 averaged over June-October, with enriched $^{18}O_p$ associated with warmer equatorial Pacific conditions). Rainfall decreases over the Maritime continent and South China Sea are consistent with enriched $^{18}O_{pw}$, since with less moist convection the water vapor is more enriched.

Discussion

Our analysis shows that $\delta^{18}O_p$-enriched years are associated with reduced summer seasonality over East Asia. This finding connects with previous interpretations of the East Asian speleothem $\delta^{18}O_c$ in that monsoon intensity, upstream depletion and source change effects all have a role to play. Monsoon intensity however plays a relatively minor role, with the latter nonlocal mechanisms being more important. However, the interpretation we advance is that the change to each process reflects the reduced summer seasonality of all processes that contribute to the climatological seasonal cycle of $\delta^{18}O_p$ over East Asia. A closer examination of what sets the East Asian $\delta^{18}O_p$ seasonal cycle will likely prove insightful.

Our analysis also connects East Asia $\delta^{18}O_p$ to the large-scale westerlies across the Tibetan Plateau. Chiang et al. (2015)[21] hypothesized that changes to the seasonal migration of the westerlies across the Plateau is responsible for East Asian paleoclimate changes. A reduced northward migration alters the timing and duration of the various rainfall intraseasonal stages - namely Spring, pre-Meiyu, Meiyu, and Midsummer - resulting in spatially complex changes to East Asian rainfall. This hypothesis has now been tested in a number of contexts spanning paleoclimate, modern, and future climates[22, 23, 24, 25]. Our result now explicitly links this hypothesis to East Asian speleothem $\delta^{18}O_c$, and adds to the growing evidence for the westerlies to play a pivotal role in East Asian summer monsoon change. Furthermore, the fact that isoGSM2 simulates the seasonal cycle of $\delta^{18}O_p$ well (compared to the other isotope-enabled models, see SI Appendix, section 1) suggests that realistic large-scale circulation fields are needed for accurate simulation of $\delta^{18}O_p$ over East Asia.

Our result ties together two seemingly unrelated lines of current research on the East Asian monsoon: the study of East Asian paleoclimate changes as informed by the speleothem oxygen isotope records, and the dynamics of the East Asian summer monsoon seasonality and the role of the jet stream. The former has revealed sizable and abrupt changes to the East Asian monsoon on centennial[26, 27], millennial[4, 28, 29, 30, 31] and orbital timescales[18, 28, 31, 32], highlighting the sensitivity of the East Asian monsoon system to climate forcings. The latter reveals a substantial and perhaps dominant role of the westerlies impinging on the Tibetan Plateau on the maintenance and change of the East Asian summer monsoon and its seasonality[12, 23, 25, 33, 34]. Our result implicates changes to the seasonal migration of westerlies across the Plateau as the dominant cause of East Asian paleomonsoon changes[21].

Materials and Methods

Isotope-incorporated Global Spectral Model version 2 (IsoGSM2): We use output from the isoGSM version 2[35] dataset over the historical period from 1979-2017. This model is an isotope-enabled (HDO and $H_2{}^{18}O$ are included) version of the Scripps Experimental Climate Prediction Center's global spectral model, that has been nudged to the National Centers for Environmental Prediction (NCEP) Reanalysis 2[36]. The nudging is done at every timestep and for all 28 sigma levels to the 6-hourly NCEP2 data, but only for temperature, zonal and meridional winds, and over large spatial scales (>1000km); in this respect it is like NCEP2 reanalysis, but with simulated isotopes. The nudging to NCEP2 allows the isoGSM2 output to be directly comparable with observations, and the simulated isotopes compare well against available observations[16]. A complete description can be found in Yoshimura et al. (2008)[16]. IsoGSM2 reproduces the seasonal cycle of precipitation and $\delta^{18}O_p$ over East Asia with fidelity when compared to observations, and is superior to isotope-enabled model simulations used in past studies of East Asia (SI Appendix, section 1). An accurate simulation of the seasonal cycle in $\delta^{18}O_p$ is crucial, as many previous interpretations relate in some way to a modulation of seasonality.

The amount-weighted annual $\delta^{18}O_p$ is the $\delta^{18}O_p$ for rainfall averaged over a calendar year (January 1 through December 31). In our analysis, we calculate the amount-weighted annual $\delta^{18}O_p$ using 6-hourly output from IsoGSM2, and assume that this value reflects the quantity chemically recorded in the cave speleothems. This assumption requires equilibrium fractionation between dripwater and precipitated calcium carbonates; we also assume that temperature-dependent fractionation effects are small. Both are commonly assumed in the climate interpretation of speleothem $\delta^{18}O_c$ (e.g. Wang et al. 2001 [4]). In most cases cave dripwater $\delta^{18}O$ approaches the annual amount-weighted value of rainwater, and the seasonal signal is damped. There is also a small seasonal effect from evaporation, that elevates the $\delta^{18}O$ in particular over the summer.

Empirical Orthogonal Function of amount-weighted annual $\delta^{18}O_p$: The dominant interannual variation of amount-weighted annual $\delta^{18}O_p$ over East Asia as simulated by isoGSM2 is extracted through an empirical orthogonal function[37] (EOF) analysis of amount-weighted annual $\delta^{18}O_p$ over East Asia [60-130°E; EQ-50°N], and standardized by subtracting the mean and dividing by the standard deviation at each location in order to isolate the effects of spatial correlation from the influence of regions of greater variance. The standardized data are then area-weighted by multiplying by the square root of the cosine of latitude prior to forming the covariance matrix. The first mode explains 14% of the total variance, and it is well separated from the other EOF modes using the criterion of North et al. (1982)[38] (SI Appendix, figure S15).

Jet position: the position of the maximum westerlies are estimated by finding, for each longitude and month, the latitude of the maximum 200mb zonal wind between 5°N and 55°N. These latitude positions are then averaged across Asia centered on the Plateau (40-140°E) to obtain the mean position for that month. The latitude of maximum wind speed is found by first interpolating the wind profile with latitude using spline interpolation (the 'spline' function in MATLAB), and then locating the maximum. If there is no peak within the 5°N-55°N range, the value is set to missing.

Data Availability: Data used in the analysis, including the monthly mean isoGSM2 data, and enriched and depleted year climatologies of isoGSM2 fields, are published and archived in Chiang et al. (2019)[39]. The Candis library[40] of analysis tools used to estimate trajectory fields for figure 4a-c, and SI Appendix, figures S13 and S14, can be found at http://kestrel.nmt.edu/~raymond/software/candis/candis.html.

Acknowledgments

This work was supported by the Department of Energy grant DE-SC0014078. The authors thank Jesse Nusbaumer, Suqin Duan, and Philip Rasch for extensive conversations about isotope-enabled climate models. Many researchers provided model output for our use in this paper, including Jung-Eun Lee (iCAM2), Camille Risi (iLMDZ), Xinyu Wen (iCAM3), Jesse Nusbaumer (iCAM5), and Clay Tabor (iCESM). Guangxin Liu and Xianfeng Wang provided the list of East Asian speleothem locations that we examined in SI Appendix, Table S2. Finally, the authors thank Wenwen Kong and Jiabin Liu for helpful conversations on East Asian monsoon dynamics, Zhaohuan Wu for assistance on the Ensemble Empirical Mode Decomposition (EEMD), and constructive comments from two reviewers.

References

1. Cheng H, Sinha A, Wang X, Cruz FW, & Edwards RL (2012) The Global Paleomonsoon as seen through speleothem records from Asia and the Americas. *Climate Dynamics* 39(5):1045-1062.
2. Wang P. X.*, et al.* (2014) The global monsoon across timescales: coherent variability of regional monsoons. *Climate of the Past* 10(6):2007.
3. Dayem KE, Molnar P, Battisti DS, & Roe GH (2010) Lessons learned from oxygen isotopes in modern precipitation applied to interpretation of speleothem records of paleoclimate from eastern Asia. *Earth and Planetary Science Letters* 295(1):219-230.
4. Wang YJ*, et al.* (2001) A high-resolution absolute-dated Late Pleistocene monsoon record from Hulu Cave, China. *Science* 294(5550):2345-2348.
5. Yuan D*, et al.* (2004) Timing, duration, and transitions of the last interglacial Asian monsoon. *Science* 304(5670):575-578.
6. Pausata FSR, Battisti DS, Nisancioglu KH, & Bitz CM (2011) Chinese stalagmite delta O-18 controlled by changes in the Indian monsoon during a simulated Heinrich event. *Nature Geoscience* 4(7):474-480.
7. Lee J-E*, et al.* (2012) Asian monsoon hydrometeorology from TES and SCIAMACHY water vapor isotope measurements and LMDZ simulations: Implications for speleothem climate record interpretation. *Journal of Geophysical Research: Atmospheres* 117(D15):D15112.
8. Maher BA (2008) Holocene variability of the East Asian summer monsoon from Chinese cave records: a re-assessment. *The Holocene* 18(6):861-866.

9. Ding Y & Chan JCL (2005) The East Asian summer monsoon: an overview. *Meteorology and Atmospheric Physics* 89(1-4):117-142.
10. Wu GX*, et al.* (2012) Thermal Controls on the Asian Summer Monsoon. *Sci Rep-Uk* 2.
11. Wu G*, et al.* (2007) The Influence of Mechanical and Thermal Forcing by the Tibetan Plateau on Asian Climate. *J. Hydrometeorol.* 8(4):770-789.
12. Molnar P, Boos WR, & Battisti DS (2010) Orographic controls on climate and paleoclimate of Asia: thermal and mechanical roles for the Tibetan Plateau. *Annual Review of Earth and Planetary Sciences* 38(1):77.
13. Schiemann R, Lüthi D, & Schär C (2009) Seasonality and Interannual Variability of the Westerly Jet in the Tibetan Plateau Region*. *Journal of Climate* 22(11):2940-2957.
14. Yeh T-C, Tao S, & Li M (1959) The abrupt change of circulation over the Northern Hemisphere during June and October. *The Atmosphere and the Sea in Motion*: *scientific contributions to the Rossby memorial volume,* Rockefeller University Press, 249-267.
15. Staff Members of the Section of Synoptic and Dynamic Meteorology, Institute of Geophysics and Meteorology, Academia Sinica, Peking (1957) On the general circulation over Eastern Asia (I). *Tellus* 9(4):432-446.
16. Yoshimura K, Kanamitsu M, Noone D, & Oki T (2008) Historical isotope simulation using reanalysis atmospheric data. *Journal of Geophysical Research: Atmospheres* 113(D19).
17. Cheng H*, et al.* (2016) The Asian monsoon over the past 640,000 years and ice age terminations. *nature* 534(7609):640.
18. Orland IJ*, et al.* (2015) Direct measurements of deglacial monsoon strength in a Chinese stalagmite. *Geology* 43(6):555-558.
19. Liu Z*, et al.* (2014) Chinese cave records and the East Asia Summer Monsoon. *Quaternary Science Reviews* 83(0):115-128.
20. Yang H, Johnson K, Griffiths M, & Yoshimura K (2016) Interannual controls on oxygen isotope variability in Asian monsoon precipitation and implications for paleoclimate reconstructions. *Journal of Geophysical Research: Atmospheres* 121(14):8410-8428.
21. Chiang JCH*, et al.* (2015) Role of seasonal transitions and westerly jets in East Asian paleoclimate. *Quaternary Science Reviews* 108:111-129.
22. Zhang H*, et al.* (2018) East Asian hydroclimate modulated by the position of the westerlies during Termination I. *Science* 362(6414):580-583.
23. Kong W, Swenson LM, & Chiang JC (2017) Seasonal transitions and the westerly jet in the Holocene east Asian summer monsoon. *Journal of Climate* 30(9):3343-3365.
24. Chiang J.C.H., Swenson L, & Kong W (2017) Role of seasonal transitions and the westerlies in the interannual variability of the East Asian summer monsoon precipitation. *Geophysical Research Letters* 44(8):3788-3795.
25. Chiang J.C.H., Fischer J, Kong W, & Herman MJ (2019) Intensification of the Pre-Meiyu Rainband in the Late 21st Century. *Geophysical Research Letters* 46(13):7536-7545.

26. Wang YJ*, et al.* (2005) The Holocene Asian monsoon: Links to solar changes and North Atlantic climate. *Science* 308(5723):854-857.
27. Zhang PZ*, et al.* (2008) A Test of Climate, Sun, and Culture Relationships from an 1810-Year Chinese Cave Record. *Science* 322(5903):940-942.
28. Wang YJ*, et al.* (2008) Millennial- and orbital-scale changes in the East Asian monsoon over the past 224,000 years. *Nature* 451(7182):1090-1093.
29. Kelly MJ*, et al.* (2006) High resolution characterization of the Asian Monsoon between 146,000 and 99,000 years BP from Dongge Cave, China and global correlation of events surrounding Termination II. *Palaeogeography, Palaeoclimatology, Palaeoecology* 236(1-2):20-38.
30. Liu Y*, et al.* (2013) Links between the East Asian monsoon and North Atlantic climate during the 8,200 year event. *Nature Geoscience* 6(2):117-120.
31. Cosford J*, et al.* (2008) East Asian monsoon variability since the Mid-Holocene recorded in a high-resolution, absolute-dated aragonite speleothem from eastern China. *Earth and Planetary Science Letters* 275(3-4):296-307.
32. Dykoski CA*, et al.* (2005) A high-resolution, absolute-dated Holocene and deglacial Asian monsoon record from Dongge Cave, China. *Earth and Planetary Science Letters* 233(1-2):71-86.
33. Park HS, Chiang JCH, & Bordoni S (2012) The Mechanical Impact of the Tibetan Plateau on the Seasonal Evolution of the South Asian Monsoon. *Journal of Climate* 25(7):2394-2407.
34. Son JH, Seo KH, & Wang B (2019) Dynamical control of the Tibetan Plateau on the East Asian summer monsoon. *Geophysical Research Letters*.
35. Yoshimura K (2015) Stable water isotopes in climatology, meteorology, and hydrology: A review. *Journal of the Meteorological Society of Japan. Ser. II* 93(5):513-533.
36. Kanamitsu M*, et al.* (2002) NCEP–DOE AMIP-II Reanalysis (R-2). *Bulletin of the American Meteorological Society* 83(11):1631-1644.
37. Weare BC & Newell R (1977) Empirical orthogonal analysis of Atlantic Ocean surface temperatures. *Quarterly Journal of the Royal Meteorological Society* 103(437):467-478
38. North, G.R., Bell, T.L., Cahalan, R.F. and Moeng, F.J., 1982. Sampling errors in the estimation of empirical orthogonal functions. *Monthly weather review*, *110*(7), pp.699-706.
39. Chiang, John; Herman, Michael; Yoshimura, Kei; Fung, Inez (2020), Data for "Enriched East Asian oxygen isotope of precipitation indicates reduced summer seasonality in regional climate and westerlies", UC Berkeley, Dataset, https://doi.org/10.6078/D1MM6B
40. Raymond DJ (1988) A C language-based modular system for analyzing and displaying gridded numerical data. *JAOT* 5(4):501-511.

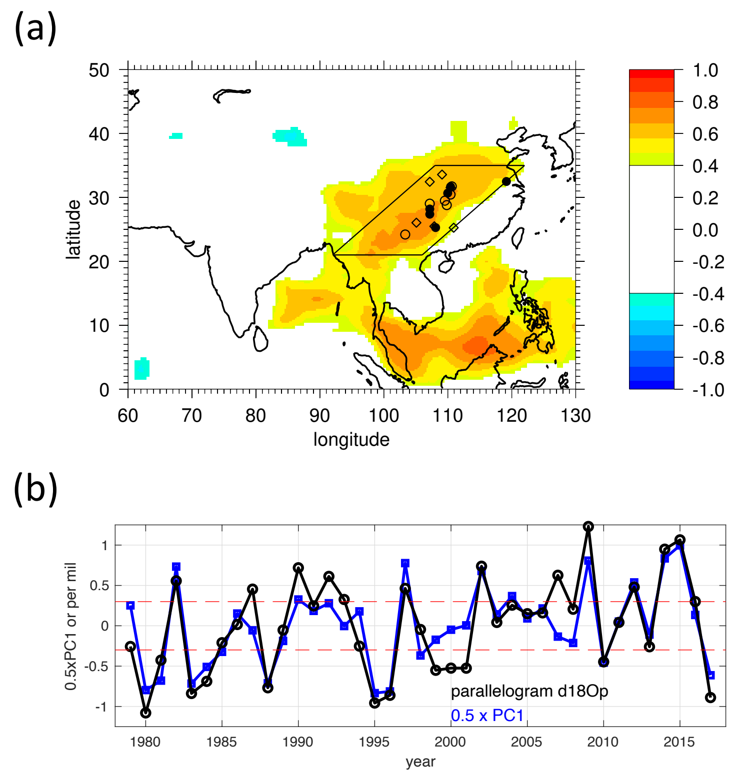

Figure 1. (a) First EOF of normalized amount-weighted annual $\delta^{18}O_p$, taken over 60-130°E and 0-50°N. The dots reference locations of speleothem records; the black filled dots are the key speleothem records of Hulu-Dongge-Sanbao, and sites with excellent coherence to these records (110.43°E, 31.67°N Sanbao; 110.42°E, 30.45°N Heshang; 119.17°E, 32.5°N Hulu; 108.08°E, 25.28°N Dongge; 109.98°E, 30.68°N Haozhu; 107.17°E, 28.18°N Shigao; 107.18°E, 27.37°N Sanxing). Caves sites with good and fair coherence with the Hulu-Dongge-Sanbao record are shown as open circles and open diamonds, respectively. See SI Appendix, section 3 for a list of these records, method of comparison, and references. The parallelogram marks the region used to generate an interrannual index of amount-weighted annual $\delta^{18}O_p$, and encompasses the region with large EOF1 loading and location of caves sites. The vertices of the parallelogram are at (anticlockwise from the bottom left point) 92°E 21°N, 106°E 21°N, 122°E 35°N, 108°E 35°N **(b)** Principal component time series of the first EOF scaled by 1/2 (blue) and average of amount-weighted annual $\delta^{18}O_p$ (units: per mil) across the parallelogram region with the mean removed (black). Dashed red lines indicate +/- 0.5 standard deviation. Black dots beyond these limits represent years comprising the enriched (N=13; above) and depleted (N=12; below) composites. The correlation coefficient between the two timeseries is $r = 0.87$ ($p < 0.01$).

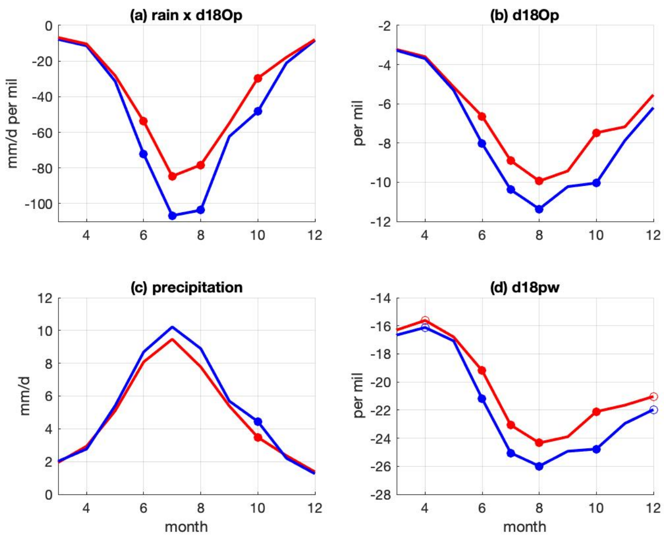

Figure 2. **(a)** Rain amount multiplied by $\delta^{18}O_p$ for each month of enriched (red) and depleted (blue) years. **(b)** Same as (a), but for $\delta^{18}O_p$. **(c)** Same as (a), but for rainfall. **(d)** Same as (a), but for $\delta^{18}O$ of precipitable water. Months where the differences in the means that are significant at $p < 0.01$ (using a 2-sided t-test) are indicated with filled circles, and those at $p < 0.05$ by open circles. While only the difference for October is significant at $p < 0.01$, the June-Oct averaged precipitation difference between enriched and depleted years is also significant at $p < 0.01$.

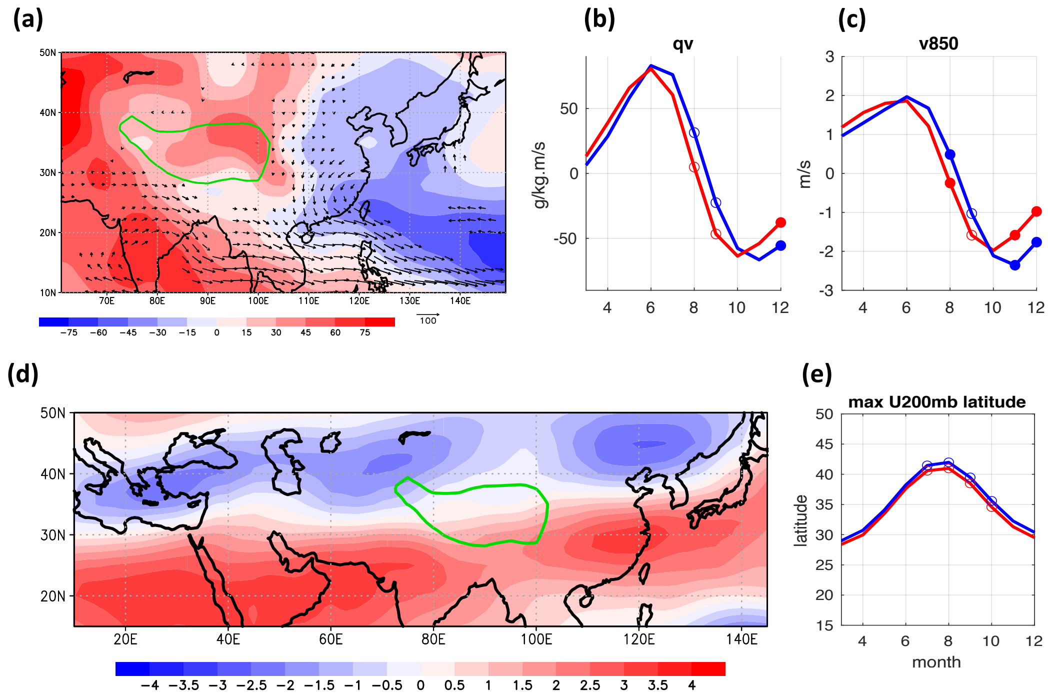

Figure 3. Seasonal changes in the atmospheric circulation. **(a)** shows the enriched minus depleted difference in JJASO vertically-integrated moisture flux (vectors) and mean sea level pressure (shaded, units in Pa). The green contour is the climatological 700mb surface pressure contour, to denote the location of the Tibetan Plateau. Only vectors for which either the zonal or meridional component is significant at $p < 0.1$ are plotted. **(b)** Vertically-integrated meridional moisture flux averaged over 105-120°E, 20-30°N for enriched (red) and depleted (blue) years. Units are kg/(m.s) (c) same as (b) but for meridional wind at 850mb; units m/s. **(d)** JJASO 200mb zonal wind, enriched minus depleted years. Units are m/s. **(e)** latitude of maximum jet speed across Asia centered on the Plateau (40-140°E) for enriched (red) and depleted (blue) years. Note that the y-axis latitude range matches that for panel (d). For (b), (c), and (e), timeseries was filtered to remove month-to-month noise prior to compositing (SI Appendix, section 4). Open circles means difference between enriched and depleted years are significant at $p < 0.05$, and filled circles at $p < 0.01$.

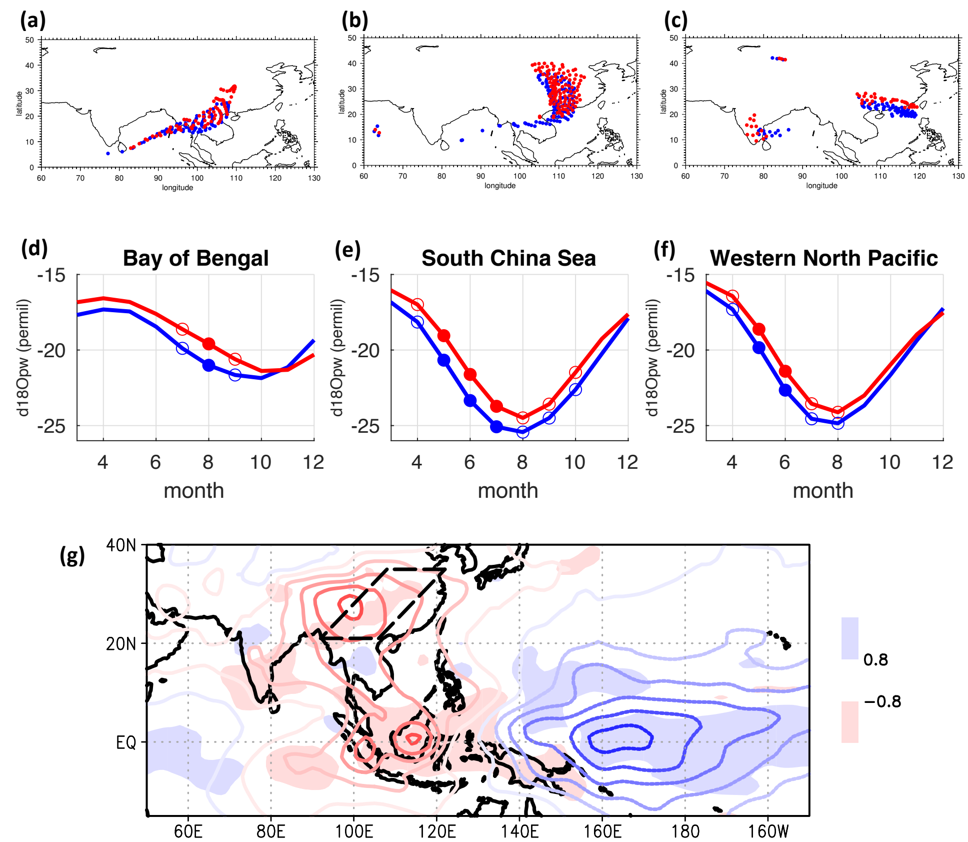

Figure 4. **(a)** July origins of trajectories that terminate in the parallelogram region at the 700mb level, as calculated using a 7-day back trajectory, for enriched years (red) and depleted years (blue). **(b-c)** same as (a), but for August and September respectively. **(d)** $\delta^{18}O_{pw}$ values averaged over the Bay of Bengal (85-95°E, 10-20°N) for enriched (red) and depleted (blue) years. Open circles means difference between enriched and depleted years are significant at $p < 0.05$, and filled circles at $p < 0.01$. **(e-f)** same as (d), but for the South China Sea (108-118°E, 12-22°N) and western North Pacific (118-128°E, 18-28°N), respectively. For (d), (e), and (f), timeseries was denoised to remove month-to-month noise prior to compositing (SI Appendix, section 4). **(g)** JJASO rainfall changes (shaded), enriched minus depleted, and JJASO $\delta^{18}O_{pw}$ enriched minus depleted (contours). The contour interval is 0.5 per mil, and negative values are dashed. The parallelogram region is marked in black dashed line for reference.